Geophysical Research Letters

RESEARCH LETTER
10.1029/2020GL087541

Global Retrievals of Solar-Induced Chlorophyll Fluorescence at Red Wavelengths With TROPOMI

Philipp Köhler[1], Michael J. Behrenfeld[2], Jochen Landgraf[3], Joanna Joiner[4], Troy S. Magney[1,5], and Christian Frankenberg[1,6]

[1]Division of Geological and Planetary Sciences, California Institute of Technology, Pasadena, CA, USA, [2]Department of Botany and Plant Pathology, Oregon State University, Corvallis, OR, USA, [3]SRON Netherlands Institute for Space Research, Utrecht, Netherlands, [4]NASA Goddard Space Flight Center, GreenbeltMD, USA, [5]Department of Plant Sciences, University of California, Davis, CA, USA, [6]Jet Propulsion Laboratory, California Institute of Technology, Pasadena, CA, USA

Key Points:
- We present the first solar-induced chlorophyll fluorescence (SIF) observations from TROPOMI at red wavelengths
- Over land, red SIF resembles the spatial distribution of far-red SIF
- Over the ocean, red SIF agrees with MODIS Fluorescence Line Height observations but provides better coverage

Supporting Information:
- Supporting Information S1

Correspondence to:
P. Köhler and C. Frankenberg,
pkoehler@caltech.edu;
cfranken@caltech.edu

Citation:
Köhler, P., Behrenfeld, M. J., Landgraf, J., Joiner, J., Magney, T. S., & Frankenberg, C. (2020). Global retrievals of solar-induced chlorophyll fluorescence at red wavelengths with TROPOMI. *Geophysical Research Letters*, *47*, e2020GL087541. https://doi.org/10.1029/2020GL087541

Received 19 FEB 2020
Accepted 4 JUL 2020
Accepted article online 17 JUL 2020

Abstract Observations of solar-induced chlorophyll *a* fluorescence (SIF) from spaceborne spectrometers can advance our understanding of terrestrial and aquatic carbon cycles. Here we present the first global retrievals of SIF at red wavelengths from the TROPOspheric Monitoring Instrument (TROPOMI). Despite the weak signal level, considerable uncertainties, and subtle measurement artifacts, spatial patterns and magnitudes agree with independent data sets. Over land, spatial patterns of our red SIF estimates covary with the far-red SIF data. Red SIF over the ocean is highly consistent with the normalized fluorescence line height (nFLH) inferred from measurements of the MODerate resolution Imaging Spectroradiometer (MODIS), even when comparing single days and fine spatial scales. Major advantages of our Fraunhofer line-based SIF retrievals include the capability to sense SIF through optically thin cloud/aerosol layers and an insensitivity to ocean color. This opens up new avenues for studying ocean biogeochemistry from space.

Plain Language Summary Plants absorb sunlight to power photosynthesis, but a small fraction of the energy is always re-emitted as a faint glow termed solar-induced chlorophyll *a* fluorescence (SIF). This weak electromagnetic signal can be measured with spectrometers that are sensitive enough and cover the wavelengths where SIF occurs (red to far red). Even though SIF is not a direct measure of the carbon uptake by photosynthesis, strong linear relationships between far-red SIF and independent estimates of photosynthesis have been observed over land. ESA's Sentinel 5 Precursor satellite hosts the TROPOspheric Monitoring Instrument (TROPOMI), a highly sensitive sensor designed to monitor atmospheric trace gases and air pollutants from space. The band setting of TROPOMI permits us also to infer SIF in both the red and far-red wavelength domain. Here, we present global estimates of red SIF over both marine and terrestrial surfaces as seen from TROPOMI.

1. Introduction

Remote sensing of biophysical parameters is key to advance our understanding of terrestrial and aquatic carbon cycling, while the need for new insights and approaches is reflected in substantial uncertainties of the global carbon budget (Beer et al., 2010; Le Quéré et al., 2018; Schimel et al., 2015). In particular, accurate knowledge about the gross primary productivity (GPP; carbon uptake) through photosynthesis is essential to inform process-based models, which are commonly used to quantify land and ocean carbon sinks. Unlike any other parameter, solar-induced chlorophyll *a* fluorescence (SIF) carries information about photosynthetic activity rather than capacity as this faint electromagnetic signal emanates during the light reactions of photosynthesis. A small fraction of the absorbed photosynthetically active radiation (PAR) is always re-emitted as SIF and has been found to covary closely with terrestrial GPP at tower sites under a wide range of environmental conditions (e.g., Guan et al., 2015; Guanter et al., 2014; Magney, Bowling, et al., 2019; Walther et al., 2016; Wood et al., 2017; Yang et al., 2015, and others). For this reason, SIF has emerged as a widely used proxy for photosynthesis in diverse terrestrial ecosystems and GPP constraint for Terrestrial Biosphere Models (Frankenberg, Fisher, et al., 2011; MacBean et al., 2018; Norton et al., 2019; Parazoo et al., 2014; Thum et al., 2017).

SIF is emitted in the red to near-infrared (NIR) spectral range (650–850 nm) with two peaks centered around 685 and 740 nm, adding a spectrally smooth signal to the reflected solar radiation, while the exact spectral shape is mostly controlled by (re)absorption effects (Erickson et al., 2019; Magney, Frankenberg, et al., 2019). For instance, the spectral reflectance of terrestrial vegetation increases rapidly in the 680–730 nm wavelength region (termed red edge), causing a selective absorption of red SIF (wavelengths <730 nm), while far-red SIF (wavelengths >730 nm) is more likely to escape the canopy. The spectral shape of SIF from terrestrial vegetation is, therefore, characterized by low magnitude, variable red SIF, and dominant, remarkably stable far-red SIF (across species and environmental conditions; Magney, Frankenberg, et al., 2019). In contrast, aquatic SIF occurs almost exclusively in the red domain (under ambient conditions), mirroring SIF emission characteristics at the chloroplast level (Buschmann, 2007). Low concentrations of phytoplankton limit the reabsorption of red SIF, while the absorption coefficient of water increases rapidly with increasing wavelength.

Concepts to decouple SIF from the total reflected light date back to the late 1970s when first aircraft observations of red SIF over water were reported (Neville & Gower, 1977). The strong and well-defined absorption characteristic of water in visible and NIR wavelengths (known as black pixel assumption) leads to a high relative contribution of red SIF to the total reflected light. This simplifies the retrieval problem to separate the SIF signal from low background reflectances (via linear interpolation in surrounding bands) after accounting for the atmospheric influence (via atmospheric correction algorithms), which can contribute over 90% to the signal at the top of atmosphere (Siegel et al., 2000). Thus, global red SIF estimates over ocean have been available for almost two decades in form of the normalized chlorophyll fluorescence line height (nFLH) estimated from the MODerate reslolution Imaging Spectroradiometer (MODIS Hoge et al., 2003; Letelier & Abbott, 1996) and the MEdium Resolution Imaging Spectrometer (MERIS Gower et al., 1999).

Remote sensing of SIF over land turned out to be more challenging (Meroni et al., 2009): Strong surface reflectance variations complicate the retrieval problem compared to measurements over water bodies. Yet the presence of distinct absorption features in the solar irradiance—solar Fraunhofer lines—enables the development of alternative retrieval strategies. SIF reduces the optical depth of solar Fraunhofer lines by affecting the central wavelength within the absorption peak in relative terms more than the continuum. Broadband spectrometers such as MERIS and MODIS are not able to resolve Fraunhofer lines, but several satellite instruments designed for atmospheric remote sensing provide a sufficient spectral resolution and signal-to-noise ratio (SNR) to exploit this effect. The first global data sets of far-red SIF over land became available in 2011 (Frankenberg, Butz, et al., 2011; Guanter et al., 2012; Joiner et al., 2011) using measurements of the Greenhouse gases Observing SATellite (GOSAT), followed by the Global Ozone Monitoring Experiment-2 (GOME-2 Joiner et al., 2013; Köhler et al., 2015), SCanning Imaging Absorption SpectroMeter for Atmospheric CHartographY (SCIAMACHY Joiner et al., 2012; Köhler et al., 2015), Orbiting Carbon Observatory-2 (OCO-2 Sun et al., 2018), TanSat Carbon Dioxide Spectrometer (Du et al., 2018), GOME (Parazoo et al., 2019), and most recently the TROPOspheric Monitoring Instrument (TROPOMI Köhler et al., 2018). To date, only two studies demonstrated the feasibility of also retrieving red SIF over terrestrial surfaces from spaceborne instruments (Joiner et al., 2016; Wolanin et al., 2015).

Here, we present a variant of an established retrieval scheme to estimate red SIF over both aquatic and terrestrial surfaces with TROPOMI. We briefly describe the instrument, outline the retrieval approach, present global red SIF observations with focus on aquatic red SIF, conduct an intersensor comparison with MODIS FLH over ocean, and discuss potentials and caveats.

2. Data and Retrieval

2.1. TROPOMI—Overview

TROPOMI's primary mission is to monitor tropospheric pollutants and greenhouse gases such as CO, CH_4, O_3, NO_2, and SO_2 with an unprecedented spatiotemporal resolution and accuracy (Veefkind et al., 2012). The host satellite, the Sentinel 5 Precursor (S-5P), was launched in October 2017 and flies in a near-polar, Sun-synchronous orbit with an equatorial crossing at 13:30 hr Local Solar Time and a ground trace repeat cycle of 17 days. The instrument's wide swath of 2,600 km provides near-daily global surface coverage with single footprints of 7 km along track (5 km since August 2019 due to reduced integration time) and 3.5–14 km across track (depending on the viewing angle). Relevant for red and far-red SIF retrievals are

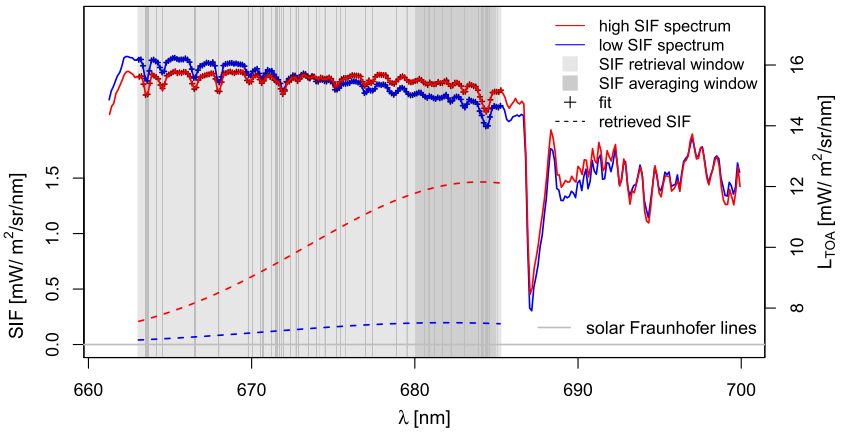

Figure 1. Two sample spectra recorded in the vicinity of Peru's coastline (locations are shown in Figure 3) with a high/low red SIF emission (red/blue). The shaded area in light gray indicates the wavelength range where the spectra are modeled (retrieval window), solar Fraunhofer line positions are displayed as vertical gray lines, model results are denoted by plus signs, and the dark gray shaded area indicates the wavelength range where the retrieved red SIF shape is averaged to report one single value.

the L1B data from TROPOMI's Bands 5 and 6, covering 661–725 and 725–775 nm with a spectral resolution of 0.38 nm.

2.2. Retrieval Approach

We implemented a variant of an established far-red SIF retrieval scheme (similar to Guanter et al., 2012, 2015; Joiner et al., 2013; Köhler et al., 2015, 2018) to estimate red SIF from TROPOMI measurements. The basic idea of such data-driven retrieval schemes consists of capturing instrument-specific features and, most importantly, the optical depth of solar Fraunhofer lines in the absence of SIF. This is achieved by sampling spectra over nonfluorescent areas (training data) and generating a set of spectral basis functions using singular value decomposition (SVD). In order to model any observation including reflectance variations and SIF, the forward model selects up to 10 eigenvectors and six Legendre Polynomials (element-wise multiplied with the first eigenvector to preserve the fractional depth of solar Fraunhofer lines), while a linear combination of two additional spectral functions represents the red SIF emission. Two spectral functions are needed to allow for wavelength shifts of the red SIF peak wavelength as well as varying slopes. For this purpose, we performed a SVD over a set of shifted Gaussians (+/−2 nm with increments of 0.1 nm) with respect to the standard red SIF approximation, a Gaussian peaking at 683 nm with a full width at half maximum of 25 nm (Abbott & Letelier, 1999). While we fit two spectral basis functions based on the SVD, we report the total red SIF emission between 680 and 685 nm, covering the red SIF peak. We chose the retrieval window ranging from 663–685.3 nm (encompassing 173 spectral points) such that telluric absorption bands (O_2-B, H_2O) and out-of-band signals are avoided, while the coverage of solar Fraunhofer lines is optimized. This way, the retrieval is relatively insensitive to atmospheric interference through trace gases, aerosols, or cloud contamination (Frankenberg et al., 2012).

Figure 1 depicts two sample spectra and retrieval results over the ocean with a low/high SIF emission (sampled from Figure 3). The impact of red SIF in such a dark scene is already noticeable as red SIF contributes up to 10% to the total signal, but it should be emphasized that the retrieval detects the emission exclusively through the changing optical depth of solar Fraunhofer lines, that is, any multiplicative effect, which might cause such curvature that looks like a SIF shape in the observed radiances would not alias into a SIF retrieval bias.

Even though terrestrial vegetation absorbs much radiation in the PAR range, reflected radiance levels are typically higher and display stronger variations compared to water bodies, which explains why we sample training spectra over land and ocean separately. Additional technical details on the selection of training spectra, retrieval algorithm, performance, and uncertainty quantification can be found in the supporting information (SI).

2.3. Quality Control, Filtering, and Uncertainty

In order to identify poor retrievals, we rely on the reduced χ^2 (statistical metric for the goodness of fit), which requires knowledge about the measurement noise/SNR. Since our SNR estimates derived from fit residuals agree with the official SNR estimates, we are confident that there are no general over/underfitting issues in the retrieval. This is also reflected in the alignment between the theoretical and empirical reduced χ^2 distribution (see the SI for details). However, several instrument-specific effects such as subtle detector nonlinearities or spectral and spatial straylight can act as an additive offset, which may be confused with the true SIF signal (Frankenberg et al., 2018; Köhler et al., 2018). Hu et al. (2018) mentioned straylight problems in TROPOMI's NIR bands, but we did not find evidence for the interference with any measurement artifacts when retrieving far-red SIF from measurements in Band 6 (Köhler et al., 2018). Here, retrievals in the vicinity of optically thick clouds often suggest strongly negative red SIF values, which is either related to straylight issues or other measurement artifacts. Those retrievals are classified as satisfactory based on the reduced χ^2 filter criteria, and some remain even when applying restrictive radiance thresholds (<50/80 mW/m^2/sr/nm over ocean/land). The restrictive filtering limits the number of valid soundings over bright surfaces including deserts and regions with frequent optically thick cloud cover but is necessary to remove potentially corrupted retrievals from the analysis. On the other hand, no explicit cloud/sun-glint filtering is needed, because low radiance levels and optically thick clouds/specular reflection are mutually exclusive.

Even though the retrieval setup complicates the uncertainty estimation, we find a strong agreement between predicted and observed uncertainties. Typical single-measurement precision errors over ocean/land are on the order of 0.3/0.5 mW/m^2/sr/nm (0.2–0.8 mW/m^2/sr/nm, depending on radiance level). The uncertainty estimates are rather conservative, as we find that actual errors are on average slightly lower than expected, which should not disguise the fact that the single-sounding uncertainty exceeds the actual red SIF signal in many cases.

3. Spatial Composites and Comparison Between TROPOMI and MODIS

The generally weak red SIF signal in combination with the high retrieval uncertainty requires aggregation of several retrievals in space and time before the data can be analyzed quantitatively. Figure 2 shows global monthly averages of red SIF over the ocean and land as well as MODIS nFLH (Behrenfeld et al., 2009) over the ocean and far-red SIF over land (Köhler et al., 2018) throughout the seasons, all gridded to a 0.2° × 0.2° spatial resolution. The MODIS instrument is flown on two satellite platforms, Aqua and Terra. Here, we focus on the MODIS-Aqua nFLH data set because of (1) very similar measurement conditions with respect to TROPOMI (ascending orbit, same overpass time, and similar swath width) and (2) radiometric instabilities and degradation of MODIS-Terra (Blondeau-Patissier et al., 2014).

Large-scale patterns of red SIF over land resemble the spatial distribution of far-red SIF with a magnitude that is roughly six times lower, which is consistent with ground-based measurements (e.g., Celesti et al., 2018; Magney, Frankenberg, et al., 2019). However, implausible features occur over central Australia, the Sahara desert, and Tibet. At the same time, those regions with bright surfaces are subject to elevated uncertainties and contain fewer valid soundings.

On the other hand, red SIF over ocean appears to be highly consistent with MODIS nFLH. Hot spots appear in regions with nutrient-rich waters (due to river discharge or upwelling), while near-zero averages can be observed in the least productive areas of the ocean. One interesting difference can be observed along China's coastline in January, where MODIS nFLH detects relatively high red SIF values and TROPOMI suggests near-zero averages. We hypothesize that the nFLH retrieval might be biased by changes in the overall ocean reflectance in these areas, where curvature in reflectance might alias into nFLH retrievals while the Fraunhofer based retrievals are insensitive to variations in the spectral shape of ocean reflectance. There are many areas with substantial differences, which warrant follow-up research beyond the scope of this manuscript.

Zonal integration of the data (right column in Figure 2) shows the radiant power of SIF per wavelength unit and degree latitude, which mitigates the potentially deceptive area distortion caused by the map projection. For example, the July composite may create the impression that higher latitudes dominate the global radiant power of far-red SIF over land, but the meridional distribution reveals a balanced contribution from high

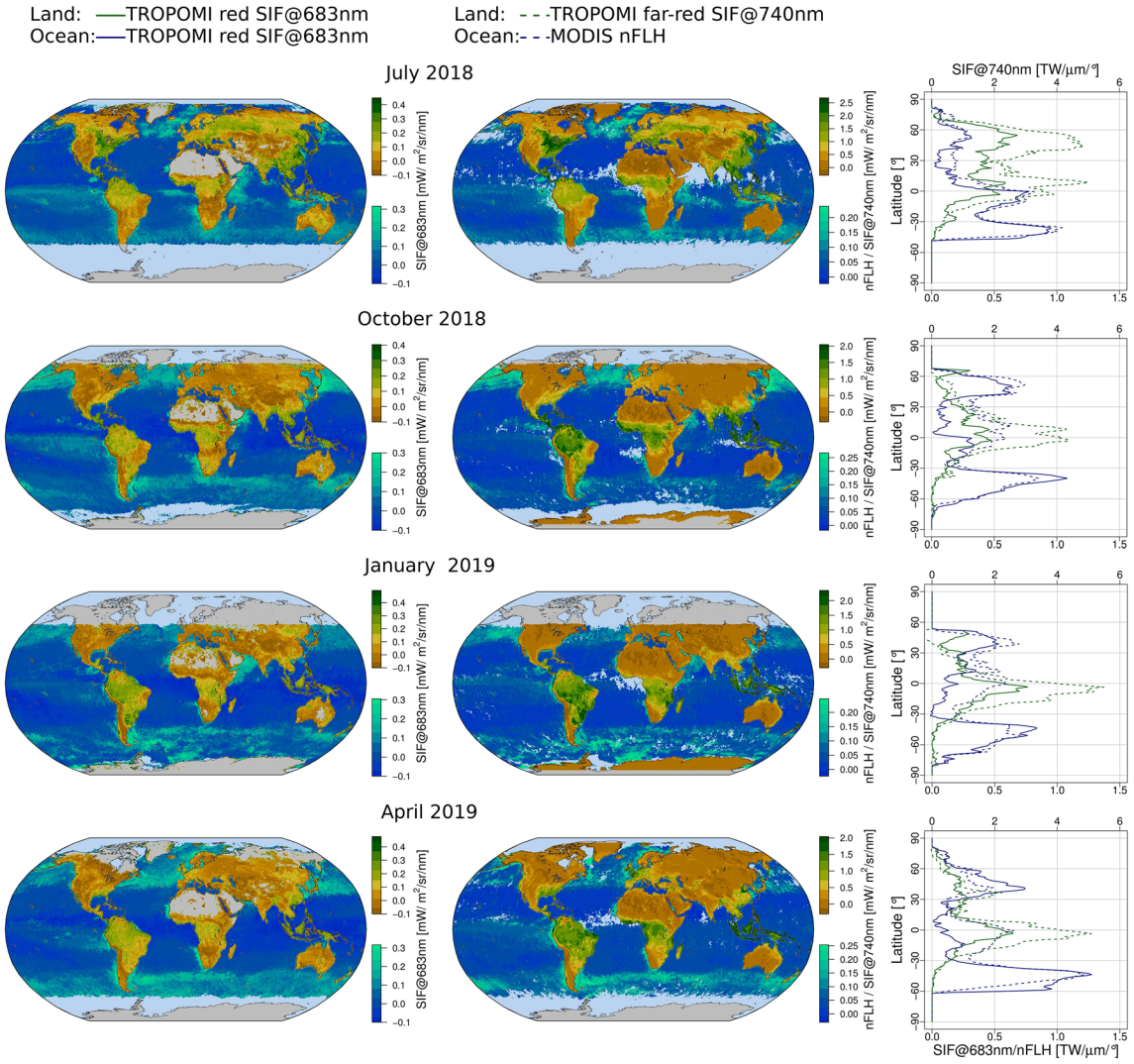

Figure 2. Monthly averages of TROPOMI red SIF over the ocean and land (left column), MODIS nFLH over the ocean and TROPOMI far-red SIF over land (middle column), and the meridional distribution of zonal integrals per degree latitude (right colunmn). A table with the global total can be found in the SI.

latitudes and the tropics. In this comparison, TROPOMI red SIF and MODIS nFLH show remarkably consistent absolute values and latitudinal variations. However, discrepancies arise around the equator where MODIS nFLH reaches a local maximum throughout the seasons, while lower TROPOMI red SIF values seem to track the shifting Inter Tropical Convergence Zone. Even though we excluded negative red SIF grid boxes from the zonal integration if the absolute value exceeds the uncertainty estimate, undetected artifacts in the TROPOMI measurements could lead to a low bias through negative red SIF estimates. In this context it should be emphasized that negative retrieval results as well as grid box averages are plausible as long as they can be explained by the measurement error. Simply removing all negative retrieval results from the analysis would inevitably lead to a high bias.

Despite minor large-scale inconsistencies and considerable single-sounding uncertainties, Figure 3 illustrates how well TROPOMI red SIF resembles MODIS nFLH at fine spatial scales (first panel) and reveals TROPOMI's improved spatial coverage (second panel). Figure 3 is of qualitative nature (we refrain from reporting actual values), because the dynamic range between the two scenes differs and the comparison is based on single TROPOMI retrieval results, which should not be overinterpreted. The Arabian Sea (second panel) is one example of where TROPOMI's improved coverage can be important as frequent harmful algae blooms occur in this sea (Do Rosário Gomes et al., 2014), while persistent cloud/areosol cover results in

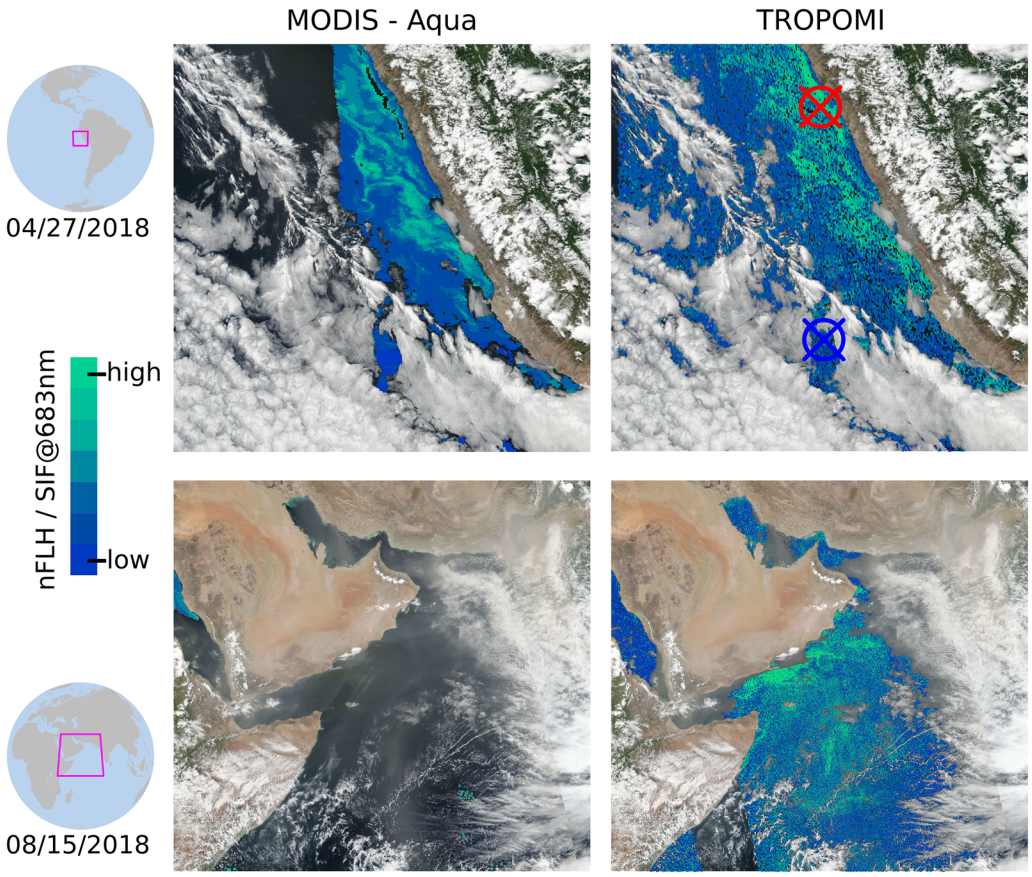

Figure 3. Comparison between MODIS nFLH and TROPOMI red SIF (single retrieval results) for two selected scenes over the upwelling zone at Peru's coastline and the Arabian Sea. Crosses in the first panel denote the location of the spectra shown in Figure 1. Note that the MODIS nFLH data coverage in the Arabian Sea is limited to a few pixel, because the retrieval requires cloud-free skies.

sparse MODIS nFLH data coverage (only a few pixels are available in the selected scene in Figure 3). This situation reflects the main benefit of solar Fraunhofer line-based SIF retrievals, which are capable of "looking through" optically thin atmospheric layers (Frankenberg et al., 2012).

To provide guidance on how TROPOMI SIF data may be analyzed on a regional scale, we highlight the Imperial Valley region in California, USA. The MODIS RGB image in the top panel of Figure 4 illustrates the strong contrasts between the Salton Sea and irrigated agriculture surrounded by desert. The spatial context is fairly well reproduced by gridding the red and far-red SIF retrievals, here shown for the entire investigated period (May 2018 to December 2019) on a $0.01° \times 0.01°$ resolution. Due to the restrictive filtering of red SIF retrievals with high radiance levels, about three times more far-red SIF retrievals are available over land. The opposite applies to the Salton Sea, where only a few soundings pass the lower radiance threshold ($20\ mW/m^2/sr/nm$) employed in the filtering of our far-red SIF retrievals, which explains why we masked the lake area in the far-red SIF map. Both the spatial context and the imbalance in the number of valid retrievals are important when generating time series as shown in the bottom panel of Figure 4.

We selected only those soundings that have an overlap of at least 90% with the lake, agriculture, or the surrounding areas to compute monthly SIF averages. In addition, red and far-red SIF retrievals over the agricultural area were colocated to ensure a fair comparison. Directional effects are assumed to cancel out through averaging 200–600 retrievals per month with a variety of viewing-illumination geometries. The extremely strong red SIF signal from the Salton Sea throughout the covered time period can be attributed to excessive algae growth promoted by nutrient intake from agricultural runoff and river discharge (Carmichael & Li, 2006). Despite the roughly sixfold weaker amplitude of red compared to far-red SIF over the agricultural

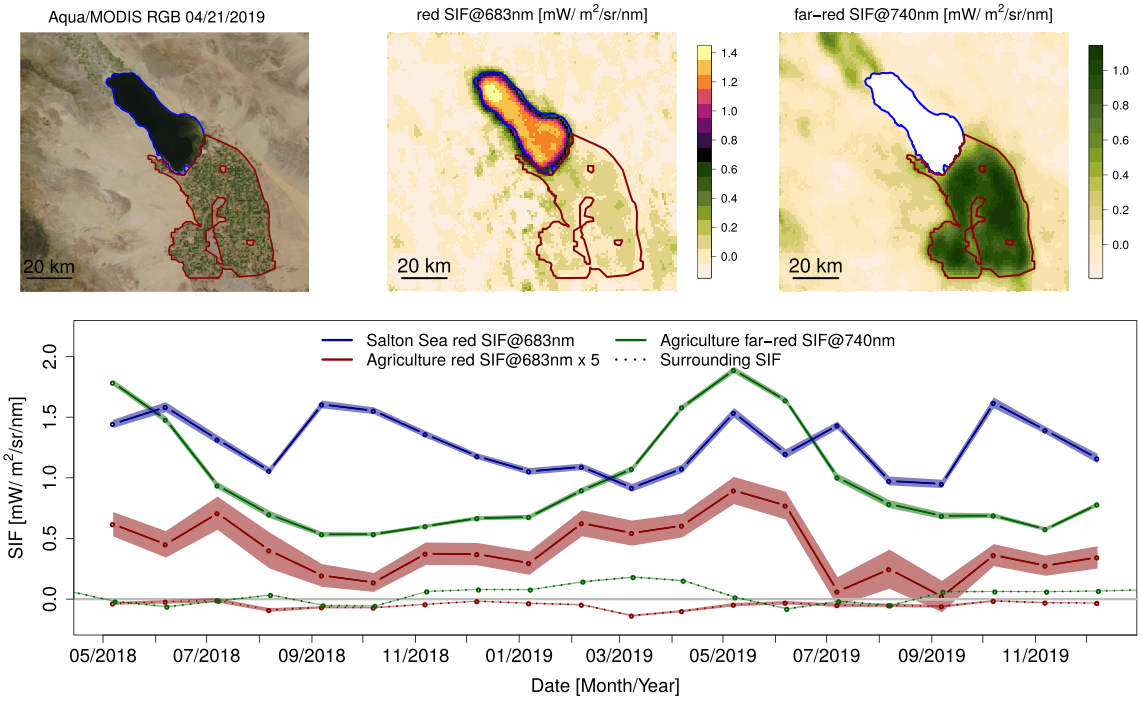

Figure 4. The top panel shows an Aqua/MODIS RGB image of the Imperial Valley in California, USA, as well as red and far-red SIF averages for the entire period under investigation (May 2018 to December 2019), gridded to a 0.01°× 0.01° resolution. The bottom panel displays monthly SIF averages and their standard error of the mean (shaded area) for soundings that have an overlap of at least 90% with of one of the contours (blue: Salton Sea; dark red: Imperial Valley agriculture excluding settlements). Note that the time series shows fivefold red SIF averages over agriculture for a better visibility of the seasonal cycle.

area, seasonal cycles covary, and some of the features in the red SIF time series may be related to canopy structural dynamics. For example, the relatively strong red SIF increase in February 2019 could be explained by reduced reabsorption of red SIF during early growing stages. However, the time series captures a mixed signal from a variety of plants, and a further analysis would require accompanying measurements. The surrounding desert is largely devoid of SIF and provides another opportunity to assess the uncertainties. We find that our red SIF single retrieval uncertainties over barren surfaces are slightly too conservative (predicted/observed: 0.55/0.38 mW/m^2/sr/nm), while the predicted and observed uncertainties for the far-red SIF retrievals match remarkably well (0.44/0.45 mW/m^2/sr/nm; see the SI for histograms).

4. Discussion

Spaceborne land/ocean remote sensing instruments provide a high spatial resolution and long time series but are not without caveats. In particular, atmospheric correction schemes are known to introduce high uncertainties in areas such as the Southern Ocean (Zeng et al., 2017). One intrinsic limitation of atmospheric satellites is the poor spatiotemporal resolution (GOME, GOME-2, and SCIAMACHY) or coverage (GOSAT and OCO-2). TROPOMI constitutes a major technological leap in this regard by approaching ecologically meaningful spatiotemporal scales, but limitations arise from high single-measurement precision errors and potentially rectifiable instrumental effects. The current radiance thresholds may become obsolete and improve the data availability if the source of the measurement artifacts interfering with our retrieval could be identified and corrected.

Over the ocean, TROPOMI red SIF provides an enhanced spatial coverage and may also serve as a tool for consistency checks, especially in regions where MODIS nFLH and TROPOMI red SIF diverge. Results over land should be treated with care, because we observe a few implausible features and higher uncertainties compared to retrievals over ocean. The generally weak red SIF signal and considerable uncertainties (especially over bright surfaces) may explain those features and reveal the need to aggregate a considerable number of measurements in space and time. However, large-scale patterns are consistent with the far-red SIF

retrievals, and our analysis on the regional scale reveals interesting features, which may be attributable to canopy structural dynamics. The observation of extremely high red SIF values over the Salton Sea has two major implications for future analyses: (1) Water bodies in the study area can have a substantial impact on time series, and (2) it demonstrates the potential of studying the seasonality of red SIF over lakes that are big enough to be captured by TROPOMI observations.

Future research may explore if the spectrally resolved red SIF emission contains information with respect to the vertical distribution of phytoplankton (Erickson et al., 2019) or canopy structure and composition. Several studies suggest that changes in chlorophyll concentrations and plant stress can be inferred from the red:far-red SIF ratio (e.g., Buschmann, 2007). In this context, it should be considered that the ratio is also controlled by the viewing-illumination geometry and canopy structure and varies on diurnal as well as seasonal time scales (Magney, Frankenberg, et al., 2019). The challenge to detect stress events by means of the red:far-red ratio will, therefore, consist of disentangling these confounding effects.

5. Conclusions

We presented the first global retrievals of red SIF from measurements of the TROPOMI instrument and compared our results to independent data sets. Over land, the spatial patterns of red SIF covary with the far-red SIF data, and the magnitude is consistent with ground-based SIF measurements. Over the ocean, TROPOMI red SIF appears to be highly consistent with the MODIS nFLH data, even when comparing single days and fine spatial scales. There is, however, some evidence for measurement artifacts resulting in negative red SIF estimates in the vicinity of optically thick clouds. Even after restrictive filtering, we can not rule out that there is a small amount of problematic soundings, which introduce a low bias in some regions. Our approach to retrieve red SIF by evaluating changes in the fractional depth of solar Fraunhofer lines is fundamentally different from the MODIS nFLH retrieval, which increases confidence in both data sets and exposes areas where further in-depth comparisons with MODIS FLH and ocean color data are warranted. In particular, the insensitivity of our retrieval to variations in the curvature of reflectance should be beneficial in situations when colored dissolved matter alters the reflectance in a way that might bias the reflectance-based nFLH approach. While dedicated spaceborne ocean color and surface vegetation remote sensing instruments arguably offer a better spatial resolution, TROPOMI observations offer the advantage of measuring SIF through optically thin cloud and aerosol layers.

Acknowledgments

This work was funded by the Earth Science U.S. Participating Investigator (Grant NNX15AH95G). M. J. B. was supported under NASA Grant Number 80NSSC18K0616. Sentinel-5 Precursor is a European Space Agency (ESA) mission implemented on behalf of the European Commission (EC). The TROPOMI payload is a joint development by ESA and the Netherlands Space Office (NSO). The Sentinel-5 Precursor ground segment development has been funded by ESA and with national contributions from the Netherlands, Germany, Belgium, and the UK. The TROPOMI SIF data can be accessed online (through ftp://fluo.gps.caltech.edu/data/tropomi/).

References

Abbott, M. R., & Letelier, R. M. (1999). Algorithm theoretical basis document chlorophyll fluorescence (MODIS product number 20). NASA (http://www.modis.gsfc.nasa.gov/data/atbd).

Beer, C., Reichstein, M., Tomelleri, E., Ciais, P., Jung, M., Carvalhais, N., et al. (2010). Terrestrial gross carbon dioxide uptake: Global distribution and covariation with climate. *Science*, *329*(5993), 834–838.

Behrenfeld, M. J., Westberry, T. K., Boss, E. S., O'Malley, R. T., Siegel, D. A., Wiggert, J. D., et al. (2009). Satellite-detected fluorescence reveals global physiology of ocean phytoplankton. *Biogeosciences*, *6*(5), 779–794.

Blondeau-Patissier, D., Gower, J. F. R., Dekker, A. G., Phinn, S. R., & Brando, V. E. (2014). A review of ocean color remote sensing methods and statistical techniques for the detection, mapping and analysis of phytoplankton blooms in coastal and open oceans. *Progress in oceanography*, *123*, 123–144.

Buschmann, C. (2007). Variability and application of the chlorophyll fluorescence emission ratio red/far-red of leaves. *Photosynthesis Research*, *92*(2), 261–271.

Carmichael, W. W., & Li, R. (2006). Cyanobacteria toxins in the Salton Sea. *Saline systems*, *2*(1), 5.

Celesti, M., van der Tol, C., Cogliati, S., Panigada, C., Yang, P., Pinto, F., et al. (2018). Exploring the physiological information of Sun-induced chlorophyll fluorescence through radiative transfer model inversion. *Remote Sensing of Environment*, *215*, 97–108.

Do Rosário Gomes, H., Goes, J. I., Matondkar, S. G. P., Buskey, E. J., Basu, S., Parab, S., & Thoppil, P. (2014). Massive outbreaks of Noctiluca scintillans blooms in the Arabian Sea due to spread of hypoxia. *Nature Communications*, *5*, 4862.

Du, S., Liu, L., Liu, X., Zhang, X., Zhang, X., Bi, Y., & Zhang, L. (2018). Retrieval of global terrestrial solar-induced chlorophyll fluorescence from TanSat satellite. *Science Bulletin*, *63*(22), 1502–1512.

Erickson, Z. K., Frankenberg, C., Thompson, D. R., Thompson, A. F., & Gierach, M. (2019). Remote sensing of chlorophyll fluorescence in the ocean using imaging spectrometry: Toward a vertical profile of fluorescence. *Geophysical Research Letters*, *46*, 1571–1579. https://doi.org/10.1029/2018GL081273

Frankenberg, C., Butz, A., & Toon, G. C. (2011). Disentangling chlorophyll fluorescence from atmospheric scattering effects in O2 A-band spectra of reflected Sun-light. *Geophysical Research Letters*, *38*, L03801. https://doi.org/10.1029/2010GL045896

Frankenberg, C., Fisher, J. B., Worden, J., Badgley, G., Saatchi, S. S., Lee, J.-E., et al. (2011). New global observations of the terrestrial carbon cycle from GOSAT: Patterns of plant fluorescence with gross primary productivity. *Geophysical Research Letters*, *38*, L17706. https://doi.org/10.1029/2011GL048738

Frankenberg, C., Köhler, P., Magney, T. S., Geier, S., Lawson, P., Schwochert, M., et al. (2018). The Chlorophyll Fluorescence Imaging Spectrometer (CFIS), mapping far red fluorescence from aircraft. *Remote Sensing of Environment*, *217*, 523–536.

Frankenberg, C., O'Dell, C., Guanter, L., & McDuffie, J. (2012). Remote sensing of near-infrared chlorophyll fluorescence from space in scattering atmospheres: Implications for its retrieval and interferences with atmospheric CO_2 retrievals. *Atmospheric Measurement Techniques*, *5*(8), 2081–2094.

Gower, J. F. R., Doerffer, R., & Borstad, G. A. (1999). Interpretation of the 685 nm peak in water-leaving radiance spectra in terms of fluorescence, absorption and scattering, and its observation by MERIS. *International Journal of Remote Sensing*, *20*(9), 1771–1786.

Guan, K., Pan, M., Li, H., Wolf, A., Wu, J., Medvigy, D., et al. (2015). Photosynthetic seasonality of global tropical forests constrained by hydroclimate. *Nature Geoscience*, *8*(4), 284–289.

Guanter, L., Aben, I., Tol, P., Krijger, J. M., Hollstein, A., Köhler, P., et al. (2015). Potential of the TROPOspheric Monitoring Instrument (TROPOMI) onboard the Sentinel-5 Precursor for the monitoring of terrestrial chlorophyll fluorescence. *Atmospheric Measurement Techniques*, *8*(3), 1337–1352.

Guanter, L., Frankenberg, C., Dudhia, A., Lewis, P. E., Gómez-Dans, J., Kuze, A., et al. (2012). Retrieval and global assessment of terrestrial chlorophyll fluorescence from GOSAT space measurements. *Remote Sensing of Environment*, *121*, 236–251.

Guanter, L., Zhang, Y., Jung, M., Joiner, J., Voigt, M., Berry, J. A., et al. (2014). Global and time-resolved monitoring of crop photosynthesis with chlorophyll fluorescence. *Proceedings of the National Academy of Sciences*, *111*(14), E1,327–E1,333.

Hoge, F. E., Lyon, P. E., Swift, R. N., Yungel, J. K., Abbott, M. R., Letelier, R. M., & Esaias, W. E. (2003). Validation of Terra-MODIS phytoplankton chlorophyll fluorescence line height. I. Initial airborne lidar results. *Applied Optics*, *42*(15), 2767–2771.

Hu, H., Landgraf, J., Detmers, R., Borsdorff, T., Aan de Brugh, J., Aben, I., et al. (2018). Toward global mapping of methane with TROPOMI: First results and intersatellite comparison to GOSAT. *Geophysical Research Letters*, *45*, 3682–3689. https://doi.org/10.1002/2018GL077259

Joiner, J., Guanter, L., Lindstrot, R., Voigt, M., Vasilkov, A. P., Middleton, E. M., et al. (2013). Global monitoring of terrestrial chlorophyll fluorescence from moderate-spectral-resolution near-infrared satellite measurements: Methodology, simulations, and application to GOME-2. *Atmospheric Measurement Techniques*, *6*(10), 2803–2823.

Joiner, J., Yoshida, Y., Guanter, L., & Middleton, E. M. (2016). New methods for the retrieval of chlorophyll red fluorescence from hyperspectral satellite instruments: Simulations and application to GOME-2 and SCIAMACHY. *Atmospheric Measurement Techniques*, *9*(8), 3939–3967.

Joiner, J., Yoshida, Y., Vasilkov, A. P., & Middleton, E. M. (2011). First observations of global and seasonal terrestrial chlorophyll fluorescence from space. *Biogeosciences*, *8*(3), 637–651.

Joiner, J., Yoshida, Y., Vasilkov, A. P., Middleton, E. M., Campbell, P. K. E., Kuze, A., & Corp, L. A. (2012). Filling-in of near-infrared solar lines by terrestrial fluorescence and other geophysical effects: Simulations and space-based observations from SCIAMACHY and GOSAT. *Atmospheric Measurement Techniques*, *5*(4), 809–829.

Köhler, P., Frankenberg, C., Magney, T. S., Guanter, L., Joiner, J., & Landgraf, J. (2018). Global retrievals of solar-induced chlorophyll fluorescence with TROPOMI: First results and intersensor comparison to OCO-2. *Geophysical Research Letters*, *45*, 10,456–10,463. https://doi.org/10.1029/2018GL079031

Köhler, P., Guanter, L., & Joiner, J. (2015). A linear method for the retrieval of Sun-induced chlorophyll fluorescence from GOME-2 and SCIAMACHY data. *Atmospheric Measurement Techniques*, *8*(6), 2589–2608.

Le Quéré, C., Andrew, R. M., Friedlingstein, P., Sitch, S., Hauck, J., Pongratz, J., et al. (2018). Global carbon budget 2018. *Earth System Science Data (Online)*, *10*(4), 2141–2194.

Letelier, R. M., & Abbott, M. R. (1996). An analysis of chlorophyll fluorescence algorithms for the Moderate Resolution Imaging Spectrometer (MODIS). *Remote Sensing of Environment*, *58*(2), 215–223.

MacBean, N., Maignan, F., Bacour, C., Lewis, P., Peylin, P., Guanter, L., et al. (2018). Strong constraint on modelled global carbon uptake using solar-induced chlorophyll fluorescence data. *Scientific Reports*, *8*(1), 1973.

Magney, T. S., Bowling, D. R., Logan, B. A., Grossmann, K., Stutz, J., Blanken, P. D., et al. (2019). Mechanistic evidence for tracking the seasonality of photosynthesis with solar-induced fluorescence. *Proceedings of the National Academy of Sciences*, *116*(24), 11,640–11,645.

Magney, T. S., Frankenberg, C., Köhler, P., North, G., Davis, T. S., Dold, C., et al. (2019). Disentangling changes in the spectral shape of chlorophyll fluorescence: Implications for remote sensing of photosynthesis. *Journal of Geophysical Research: Biogeosciences*, *124*, 1491–1507. https://doi.org/10.1029/2019JG005029

Meroni, M., Rossini, M., Guanter, L., Alonso, L., Rascher, U., Colombo, R., & Moreno, J. (2009). Remote sensing of solar-induced chlorophyll fluorescence: Review of methods and applications. *Remote Sensing of Environment*, *113*(10), 2037–2051.

Neville, R. A., & Gower, J. F. R. (1977). Passive remote sensing of phytoplankton via chlorophyll α fluorescence. *Journal of Geophysical Research*, *82*(24), 3487–3493.

Norton, A. J., Rayner, P. J., Koffi, E. N., Scholze, M., Silver, J. D., & Wang, Y.-P. (2019). Estimating global gross primary productivity using chlorophyll fluorescence and a data assimilation system with the BETHY-SCOPE model. *Biogeosciences*, *16*(15), 3069–3093.

Parazoo, N. C., Bowman, K., Fisher, J. B., Frankenberg, C., Jones, D., Cescatti, A., et al. (2014). Terrestrial gross primary production inferred from satellite fluorescence and vegetation models. *Global Change Biology*, *20*(10), 3103–3121.

Parazoo, N. C., Frankenberg, C., Köhler, P., Joiner, J., Yoshida, Y., Magney, T., et al. (2019). Towards a harmonized long-term spaceborne record of far-red solar-induced fluorescence. *Journal of Geophysical Research: Biogeosciences*, *124*, 2518–2539. https://doi.org/10.1029/2019JG005289

Schimel, D., Pavlick, R., Fisher, J. B., Asner, G. P., Saatchi, S., Townsend, P., et al. (2015). Observing terrestrial ecosystems and the carbon cycle from space. *Global Change Biology*, *21*(5), 1762–1776.

Siegel, D. A., Wang, M., Maritorena, S., & Robinson, W. (2000). Atmospheric correction of satellite ocean color imagery: The black pixel assumption. *Applied optics*, *39*(21), 3582–3591.

Sun, Y., Frankenberg, C., Jung, M., Joiner, J., Guanter, L., Köhler, P., & Magney, T. (2018). Overview of solar-induced chlorophyll fluorescence (SIF) from the Orbiting Carbon Observatory-2: Retrieval, cross-mission comparison, and global monitoring for GPP. *Remote Sensing of Environment*, *209*, 808–823.

Thum, T., Zaehle, S., Köhler, P., Aalto, T., Aurela, M., Guanter, L., et al. (2017). Modelling sun-induced fluorescence and photosynthesis with a land surface model at local and regional scales in northern Europe. *Biogeosciences*, *14*(7), 1969.

Veefkind, J. P., Aben, I., McMullan, K., Förster, H., De Vries, J., Otter, G., et al. (2012). TROPOMI on the ESA Sentinel-5 Precursor: A GMES mission for global observations of the atmospheric composition for climate, air quality and ozone layer applications. *Remote Sensing of Environment*, *120*, 70–83.

Walther, S., Voigt, M., Thum, T., Gonsamo, A., Zhang, Y., Köhler, P., et al. (2016). Satellite chlorophyll fluorescence measurements reveal large-scale decoupling of photosynthesis and greenness dynamics in boreal evergreen forests. *Global Change Biology*, *22*(9), 2979–2996.

Wolanin, A., Rozanov, V. V., Dinter, T., Noël, S., Vountas, M., Burrows, J. P., & Bracher, A. (2015). Global retrieval of marine and terrestrial chlorophyll fluorescence at its red peak using hyperspectral top of atmosphere radiance measurements: Feasibility study and first results. *Remote Sensing of Environment*, *166*, 243–261.

Wood, J. D., Griffis, T. J., Baker, J. M., Frankenberg, C., Verma, M., & Yuen, K. (2017). Multiscale analyses of solar-induced florescence and gross primary production. *Geophysical Research Letters*, *44*, 533–541. https://doi.org/10.1002/2016GL070775

Yang, X., Tang, J., Mustard, J. F., Lee, J.-E., Rossini, M., Joiner, J., et al. (2015). Solar-induced chlorophyll fluorescence that correlates with canopy photosynthesis on diurnal and seasonal scales in a temperate deciduous forest. *Geophysical Research Letters*, *42*, 2977–2987. https://doi.org/10.1002/2015GL063201

Zeng, C., Zeng, T., Fischer, A., & Xu, H. (2017). Fluorescence-based approach to estimate the chlorophyll-a concentration of a phytoplankton bloom in Ardley Cove (Antarctica). *Remote Sensing*, *9*(3), 210.